



ELSEVIER

Contents lists available at ScienceDirect

## Opto-Electronics Review

journal homepage: <http://www.journals.elsevier.com/opto-electronics-review>

# SU-8 based planar metamaterials with fourfold symmetry as selective terahertz absorbers

B. Grześkiewicz<sup>a</sup>, A. Sierakowski<sup>b</sup>, J. Marczewski<sup>b</sup>, N. Pałka<sup>c</sup>, E. Wolarz<sup>a,\*</sup>

<sup>a</sup> Faculty of Technical Physics, Poznan University of Technology, 3 Piotrowo St., 60-965 Poznan, Poland

<sup>b</sup> Institute of Electron Technology, 32/46 Al. Lotnikow, 02-668 Warsaw, Poland

<sup>c</sup> Institute of Optoelectronics, Military University of Technology, 2 Urbanowicza St., 00-908 Warsaw, Poland

## ARTICLE INFO

## Article history:

Received 25 May 2018

Received in revised form 15 October 2018

Accepted 27 October 2018

Available online 22 November 2018

## Keywords:

Terahertz metamaterial absorber

Terahertz spectroscopy

Transmittance

Reflectance

## ABSTRACT

We report on the absorption properties of polarization-insensitive transmissive and reflective metamaterial absorbers based on two planar aluminium periodic structures and SU-8 epoxy resist. These absorbers were investigated using numerical simulation and experimental methods in the terahertz range (below 2 THz). SU-8 is a very promising organic material for dielectric layers in planar metamaterials, because its application simplifies the process of fabricating these structures and significantly reduces the fabrication time. The experimental absorption of the metamaterial absorbers has narrowband characteristics that were consistent with the numerical simulations. Power flow analysis in the transmissive metamaterial unit cell shows that the absorption in the terahertz range occurs primarily in the SU-8 layer of the absorber.

© 2018 Association of Polish Electrical Engineers (SEP). Published by Elsevier B.V. All rights reserved.

## 1. Introduction

The term “metamaterials” is used in relation to artificial composite materials with a periodic internal structure [1]. Metamaterials are characterized by electromagnetic properties not found in nature. By definition, dimensions of the unit cells of metamaterials are many times smaller than the length of electromagnetic waves in the frequency range in which the unusual electromagnetic properties are observed. This applies in particular to microwave, millimetre, terahertz, and medium and near infrared ranges, as well as to the visible range. Of particular interest are metamaterials with electromagnetic response in the so-called “terahertz gap” which extends from 0.1 THz to 10 THz [2]. In this frequency range, the electromagnetic response of natural materials, arising from interactions with electrons in localized states or delocalized electrons in bands, is relatively weak.

Since the first terahertz metamaterials were fabricated, many of their various functionalities have been presented. In particular, this applies to terahertz metamaterial absorbers (TMAs) characterized by a close-to-unity absorption of electromagnetic radiation [3,4]. As a general principle, TMAs are planar metal-dielectric-

metal structures [5,6]. The metal layers of TMAs, separated by a dielectric layer, have a periodic structure created from unit cells responsible for characteristic electromagnetic resonances. Because of the characteristic symmetry of the unit cells, TMAs are sensitive to the polarization of electromagnetic wave [6,7]. In the special case where the unit cell of a planar TMA has a four-fold rotational symmetry about the axis normal to the surface, the metamaterial absorber is insensitive to the polarization of the incident electromagnetic waves [8–10].

In addition to the single-band designs, dual band [11–13], multiband [14–16], and broadband TMAs [17–19] have also been reported. The absorption properties of a TMA are related to the shape of the unit cell, its size, and the type of materials used to construct it. In particular, thickness of the separating layer and its dielectric properties have a significant influence on the parameters of the TMA absorption band [20]. The electromagnetic properties of TMAs can also be dynamically modified, e.g., by using liquid crystal layers [21]. TMAs can be used as active elements in sensors for detecting biological materials [22], organic compounds [23], and explosives in the security technology [24]. Perfect TMAs are also good candidates for applications as efficient antennas in terahertz detectors based on field effect transistors [25] or as very sensitive bolometers [26].

Numerical simulation methods based on Maxwell's equations are currently the most commonly used methods in the design of metamaterial absorbers. For a metamaterial structure treated as a homogeneous medium, these methods allow for a determination of

\* Corresponding author.

E-mail addresses: [bartekgrzes85@gmail.com](mailto:bartekgrzes85@gmail.com) (B. Grześkiewicz), [asierak@ite.waw.pl](mailto:asierak@ite.waw.pl) (A. Sierakowski), [jmarcz@ite.waw.pl](mailto:jmarcz@ite.waw.pl) (J. Marczewski), [norbert.palka@wat.edu.pl](mailto:norbert.palka@wat.edu.pl) (N. Pałka), [eryk.wolarz@put.poznan.pl](mailto:eryk.wolarz@put.poznan.pl) (E. Wolarz).

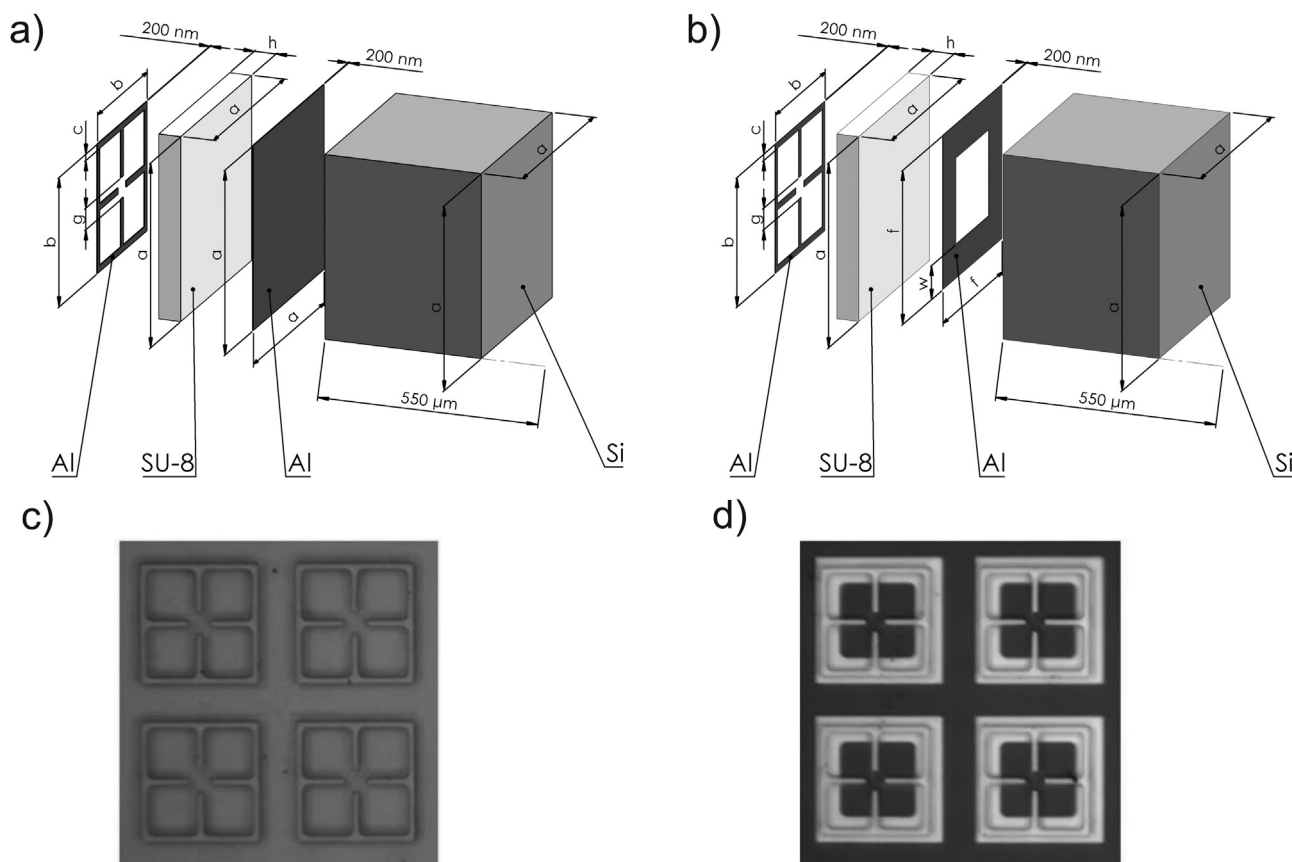


**Fig. 1.** The designs of unit cells and microscope images of reflective (a, c) and transmissive (b, d) TMAs ( $a = 60 \mu\text{m}$ ,  $b = 42 \mu\text{m}$ ,  $c = 2 \mu\text{m}$ ,  $h = 7 \mu\text{m}$ ,  $f = 50 \mu\text{m}$ ,  $g = 7 \mu\text{m}$ ,  $w = 11 \mu\text{m}$ ).

the coefficients of the dispersion matrix, the so-called S-parameters [27]. The conditions of perfect absorption are obtained by matching the wave impedance of the metamaterial to the wave impedance of the environment. On the basis of S-parameters, electric permittivity and magnetic permeability of the metamaterial can be determined [28–30]. As a consequence, it is possible to gain an insight into the physical nature of the processes of absorption and scattering of energy associated with the electromagnetic field in the metamaterial structure.

The dielectric layer found in terahertz metamaterials plays a dual role as a structural material and as a material with a defined electrical permeability. Dielectric layers from inorganic materials, e.g.  $\text{SiO}_2$ , meet the above conditions but their deposition usually requires the use of complicated and expensive techniques. For this reason, at the cost of lowering thermal resistance, inorganic materials are replaced with organic materials, such as, for example, benzocyclobutene (BCB) [31] or epoxy based photoresists [32]. The SU-8 epoxy resist, which has been widely used as a structural material for MEMS devices [33], is a very promising material for the fabrication of metal-organic terahertz metamaterial structures [10,32,34]. A dielectric layer made of SU-8, in addition to its basic function of separating the metal layers, also ensures high mechanical stability of the metamaterial structure. Deposition techniques applied to SU-8 are relatively simple and rapid, which results in a significant reduction in the metamaterial absorber fabrication costs.

In this paper, we discuss the absorption properties of reflective and transmissive terahertz metamaterial absorbers based on SU-8 epoxy resist. A common feature of these two types of absorbers is the use of identical elementary metal resonators forming the outer layer of the metamaterial structures. The absorbers were designed by using numerical simulations and subsequently fabricated by a

multi-step lithography process. Reflection and transmission of the absorbers were measured by using terahertz time-domain spectroscopy, and the results were then compared with the results of numerical simulations. The S-parameters were simulated at external planes commonly called ports. We have modified the standard mathematical formulas defining S-parameters for planar metamaterial to take into account port distances from the outside surfaces of the absorbers. These distances should be as short as possible, but large enough so that the near field is negligible on the ports. This problem was identified earlier, but was not always factored in the calculations [28,29]. We also calculated effective electromagnetic parameters of the absorbers, such as, wave impedance, refractive index, permittivity, and permeability. We apply the determined permittivity and permeability to the analysis of electromagnetic field energy absorption inside the unit cells of the transmissive absorbers.

## 2. Design and fabrication of terahertz metamaterial absorber

Designs of unit cells of the investigated reflective and transmissive TMAs, as well as their images obtained using a metallographic microscope are presented in Fig. 1. In our case, the TMAs were designed as two-layer aluminium structures separated by a thin dielectric layer of SU-8 epoxy-based resist and deposited on the surface of high-resistivity silicon. The unit cell has a four-fold symmetry with respect to the axis normal to the surface of the absorber. According to the principles of optics, a linearly polarized electromagnetic wave falling perpendicular to the surface of the optically uniaxial metamaterial is divided into two waves travelling along the fourfold symmetry axis. The electric vectors of these waves are parallel to the perpendicular edges of the unit cell. Due to the sym-

metry of the structure, both waves are weakened in the same way and they also show the same phase shift inside the metamaterial. Then, after passing through the medium they are re-assembled into a single wave with polarization identical to the polarization of the incident wave. It follows from the principle of projecting the electric wave vector to the directions determined by edges of the unit cell that intensity of the passing (or reflected) terahertz wave does not depend on polarization of the wave incident perpendicular to the surface. This principle has been previously tested experimentally for a similar metamaterial structure and in the same experimental conditions as currently [10].

The outer metal layers in the reflective and transmissive TMAs are formed by networks of identical square-shaped resonators with the same lattice constants. In the transmissive TMA, the inner metal layer is composed of four cut-wires connected in a square layout, whereas in the reflective TMA, a uniform Al layer is used. The investigated TMAs are two-dimensional structures with lattice constants equal to 60  $\mu\text{m}$ . The thickness of the metal layers is of 200 nm and the size of the smallest resonator details is about 2  $\mu\text{m}$ . The SU-8 spacer and the Si substrate are 7  $\mu\text{m}$  thick and about 550  $\mu\text{m}$  thick, respectively. The arrays of the cut-wire structures in the inner layer and the squared resonators in the outer interface of TMAs were produced using metal evaporation and standard high-precision photolithography techniques. The desired thickness of SU-8 spacer on the ground Si substrate with the uniform Al layer or the cut-wire structures was achieved through calibrated control of the ST-146 (CONVAC) spinner rotation in accordance with the manufacturer's (MicroChem) instructions. The SU-8 spacer was soft-baked for 2 min at 95  $^{\circ}\text{C}$  and next polymerized by exposing it to UV light with the use of a long pass filter to eliminate UV radiation below 350 nm. Exposure to UV was about 150  $\text{mJ}/\text{cm}^2$ . Finally, the SU-8 layer was subjected to a two-stage post exposure baking: for 1 min at 65  $^{\circ}\text{C}$ , then for 2 min at 95  $^{\circ}\text{C}$ .

The prepared metamaterial samples whose dimensions are about 5 mm by 4 mm contain approximately 5000 elementary resonators arranged in 80 rows and 60 columns. More than 100 metamaterial samples were obtained from one silicon wafer having a standard diameter of 40 mm.

### 3. Numerical simulation method

Transmittance, reflectance, and absorption spectra of the investigated metamaterial absorbers were obtained from numerical simulations for a single metamaterial cell using CST Microwave Studio commercial software. The Fabry-Pérot interference pattern of the thick Si substrate (étalon) was observed in the simulated curves. This effect was regarded as irrelevant to the problem being considered here; consequently, the interference pattern was removed numerically from simulated curves by deleting the higher-order Fourier components.

Transmittance and reflectance of a plane wave incident on a homogenous metamaterial slab can be characterized by a  $2 \times 2$  scattering matrix  $[S_{ij}]$  with complex components called S-parameters [27]. The  $S_{11}$  parameter is the ratio of electric (or magnetic) field amplitudes of the wave reflected from one side of the slab and the incident wave. The corresponding matrix component for the opposite side of the metamaterial plate is given by  $S_{22}$ . The  $S_{21}$  and  $S_{12}$  parameters are the ratios of electric (or magnetic) field amplitudes of waves passing through the slab forward and backward, respectively, to the amplitudes of the incident waves. The S-parameters can be determined experimentally or simulated numerically on the basis of Maxwell's equations. Complex S-parameters are related to complex wave impedance and refractive index [28–30]. We have modified the standard formulas to

include in them the port distances from the outside surfaces of the planar metamaterial absorbers as follows:

$$S_{21} = e^{in_{s1}kd_1} e^{in_{s2}kd_2} \frac{[1 - (Z - 1)^2(Z + 1)^{-2}] e^{inkd}}{1 - (Z - 1)^2(Z + 1)^{-2} e^{2inkd}}, \quad (1a)$$

$$S_{11} = e^{2in_{s1}kd_1} \frac{(Z - 1)(Z + 1)^{-1} (1 - e^{2inkd})}{1 - (Z - 1)^2(Z + 1)^{-2} e^{2inkd}}, \quad (1b)$$

where  $d$  is the thickness of the metamaterial slab,  $d_1$  and  $d_2$  are the distances between the slab walls and the ports at which the electric (or magnetic) fields of the waves are measured,  $n_{s1}$  and  $n_{s2}$  are the refractive indices of the medium in front of the sample and at the back, respectively,  $k$  is the wave number in free space, and  $i$  is the imaginary unit.

The location of the ports at which the S-parameters are calculated has an influence on the results of simulations and, consequently, on the effective electromagnetic parameters of the TMAs. In order to minimize the contribution of the near-field to the electromagnetic field of travelling waves, numerical simulations were performed for planar ports located within a distance of 12  $\mu\text{m}$  from both the outer metal resonator and the external boundary of a Si layer. The assumed distance between the absorbers and the ports was as small as possible to minimize contributions to the parameters introduced by surrounding media (air). For numerical simulations, the real part of permittivity and loss factor ( $\tan \delta$ ) of the high-resistivity Si were taken as 11.68 and 0.01, respectively, at 1 THz [35]. For SU-8, and at the same frequency, these parameters were assumed to be equal to 2.75 and 0.14, accordingly. These values for SU-8 were chosen so as to achieve agreement between frequency positions of the experimental and simulated absorption maxima. The assumed value of the real part of permittivity for SU-8 differs from the published value, which equals 2.89 [36,37].

Frequency dependence of the wave impedance  $Z$  and the refractive index  $n$ , as well as the electric permittivity  $\epsilon$  and the magnetic permeability  $\mu$  can be calculated from Eqs. (1a) and (1b), which are generally valid for isotropic media and can be also used for anisotropic media if the electromagnetic waves propagate along the principal axes. If the scattering of the electromagnetic waves in a metamaterial is neglected, then the absorption can be calculated from S-parameters by using equation:

$$A = 1 - T - R, \quad (2)$$

where  $T = |S_{21}|^2$  and  $R = |S_{11}|^2$  are the transmittance and reflectance, respectively.

### 4. Experimental

TMAs were checked for defects in the metal structures using a metallographic microscope, and then the selected samples without defects were verified for repeatability of transmission and reflection spectra in the terahertz range. It was found that some imperfections in the metal structures could affect the resonance frequency. However, defects in the structures have less effect on resonances than the inaccuracy in thickness of the dielectric SU-8 layer. The manufacturing process guarantees that inaccuracy in this parameter is less than 3%. For the transmissive TMA [Fig. 1a) and c)], both reflectance and transmittance spectra were measured, whereas for the reflective absorber [Fig. 1b) and d)], only the reflectance spectrum was obtained, because transmission equals zero over the entire frequency range.

Experimental transmittance, reflectance, and absorption spectra for the investigated TMAs were obtained for samples consisting of many unit cells. The spectra were measured using a TPS 3000 (Teraview) terahertz time-domain spectrometer purged with dry air. The spectral range of terahertz pulse generated in the spec-

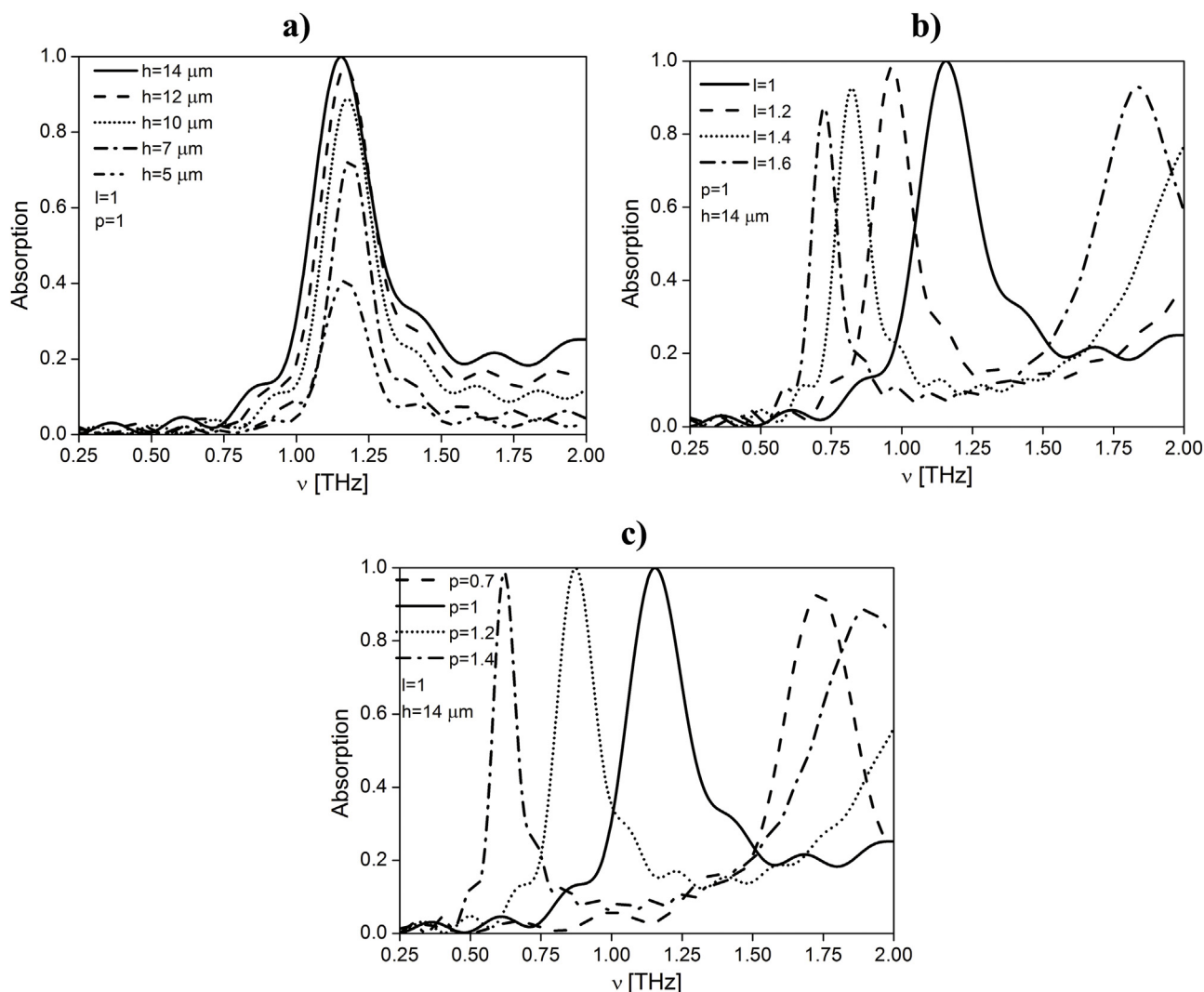


**Fig. 2.** Simulated absorption of reflective TMA for different thickness  $h$  of SU-8 layer at constant scaling factors  $l$  and  $p$  ( $l = p = 1$ ) (lines:  $h = 14 \mu\text{m}$  – solid,  $h = 12 \mu\text{m}$  – dashed,  $h = 10 \mu\text{m}$  – dotted,  $h = 7 \mu\text{m}$  – dash-dotted,  $h = 5 \mu\text{m}$  – dash-double-dotted) a), for different  $l$  scaling factors of metal structure at constant  $p$  and  $h$  ( $p = 1$ ,  $h = 14 \mu\text{m}$ ) (lines:  $l = 1$  – solid,  $l = 1.2$  – dashed,  $l = 1.4$  – dotted,  $l = 1.6$  – dash-dotted) b), and for different  $p$  scaling factor of lattice parameter and constant  $l$  and  $h$  ( $l = 1$ ,  $h = 14 \mu\text{m}$ ) (lines:  $p = 0.7$  – dashed,  $p = 1$  – solid,  $p = 1.2$  – dotted,  $p = 1.4$  – dash-dotted) c).

trometer was from 0.1 THz to 3.0 THz. The terahertz pulse was transmitted through the sample (for the transmissive absorber) or reflected from its surface (for both transmissive and reflective absorbers), and then it was detected by a terahertz antenna gated by the probe beam. The signal was measured using a lock-in amplifier, and then the data were processed using a computer with dedicated software. Transmittance was recorded for the pulse incident perpendicular to the sample surface, with dry air as the reference. The gradually decreasing multiple reflections in a thick Si substrate were cut from the signal to exclude interference fluctuations from transmittance spectra. Thus, these spectra included information about electromagnetic response of the metal-dielectric structure. Reflectance was measured for the incidence angle of a pulse equal to  $22.5^\circ$  which was associated with the limitations of the apparatus. The error introduced in the reflectance by this oblique incidence, estimated based on the Fresnel equations, was less than 1%. The frequency dependence of transmittance and reflectance was obtained using the Fourier transform of the electric signal. Additional details of the experimental setup and the measurement method are given elsewhere [10].

## 5. Reflective terahertz metamaterial absorbers

The effects of SU-8 dielectric layer thickness, as well as size of the metal structure and lattice constant on absorption of the reflective TMA, are shown in Fig. 2. For ease of discussion,  $l$  and  $p$  scaling factors are defined, correspondingly, as ratios of the metal structure dimensions and the lattice parameter of the considered TMAs cells to those of the fabricated reflective TMA (Fig. 1) but with thicker dielectric layer ( $h = 14 \mu\text{m}$ ). It can be seen that thickness of the SU-8 layer has a significant influence on absorption at the peak [Fig. 2a]. By varying the dielectric layer thickness,  $h$ , in the range from  $5 \mu\text{m}$  to  $14 \mu\text{m}$ , the absorber can be matched for both high peak absorption and high Q-factor. It is evident that the condition of perfect absorber is satisfied for the SU-8 layer with a thickness equal to  $14 \mu\text{m}$ .

The absorption peak position can be also effectively controlled by scaling size of the metal structures by  $l$  factor at a constant lattice parameter [Fig. 2b]) or by scaling the lattice parameter by  $p$  factor at constant dimensions of the metal structures [Fig. 2c]). Figure 2b) shows that the increase in  $l$  factor by 60% corresponds to the shift

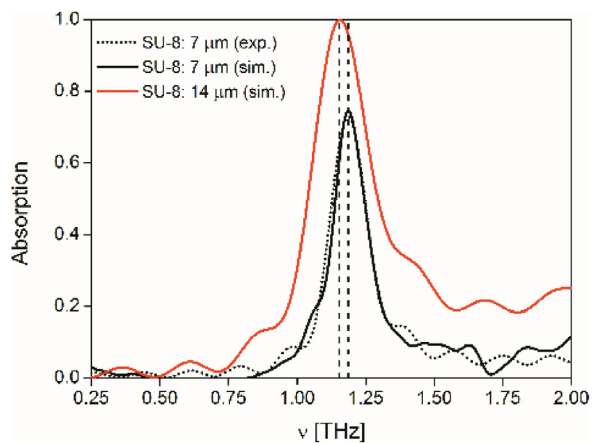


**Fig. 3.** Absorption spectra of a reflective TMA with a 7  $\mu\text{m}$  thick SU-8 layer obtained experimentally (black dotted line) and simulated numerically (black line), and the spectrum simulated numerically for a reflective perfect TMA with a 14  $\mu\text{m}$  thick SU-8 layer (red line).

of the absorption peak towards lower frequencies by more than 0.5 THz and, simultaneously, a 1.9 times increase of Q-factor up to a value of 6.5. An analogous correlation between  $p$  factor and the absorption peak position is observed in Fig. 2c). In this case, the increase in  $p$  factor by 40% corresponds to a 1.8 times increase of Q-factor up to a value of 6.4.

Figure 3 shows the absorption spectra of reflective TMAs obtained from the experimental and numerical simulations. Absorption is calculated from the reflectance  $R$  under the assumption that transmittance  $T=0$ . The spectra are simulated for a unit cell having the same dimensions and electrical parameters as those of the fabricated sample. For comparison, the figure also shows the results of simulations for a unit cell of a reflective perfect TMA whose SU-8 layer is 14  $\mu\text{m}$  thick; in this case,  $A=1$  at the peak maximum. This thickness is twice the thickness of the layer in the fabricated TMA. It can be seen that the experimental absorption spectrum is consistent with the spectrum simulated for the TMA cell with the same geometrical and electrical parameters. The maximum value of the experimental absorption, equal to 0.75, occurs at 1.18 THz, the half-width of the absorption peak is of 0.17 THz, and the Q-factor has a value of 6.9. For the perfect TMA, the absorption maximum is shifted toward lower frequencies relative to the fabricated absorber and is found at 1.15 THz. The half-width and Q-factor of the absorption peak for the perfect TMA are equal to 0.25 THz and 4.6, respectively. Two absorption spectra obtained from the numerical simulations show that the increase of the peak value of absorption is associated with the decrease in Q-factor.

Figure 4 presents the wave impedance  $Z$  as a function of frequency for two simulated reflective TMAs. One of them has the same dimensions as the fabricated TMA and the other is a reflective perfect TMA. The  $S_{21}$  parameter for a reflective TMA is equal to zero by definition. For TMAs, the condition of perfect absorption at a given frequency is formally written as  $S_{11}=0$ . Then, according to Eqs. (1a) and (1b),  $Z_1=1$  and  $Z_2=0$  for the real and imaginary parts of wave impedance, respectively. As can be seen in Fig. 4, these conditions are satisfied for the perfect TMA (i.e., the one whose SU-8 thickness was of 14  $\mu\text{m}$ ) at a frequency of 1.15 THz. This frequency value fits well to the maximum of the absorption peak (Fig. 3). On the other hand, for the reflective TMA with a 7  $\mu\text{m}$  thick SU-8 layer, the dispersion region of wave impedance is shifted toward higher frequencies. In this case,  $Z_1 < 1$  and  $Z_2 < 0$  over the entire tested frequency range, which means that this absorber is not a perfect one.

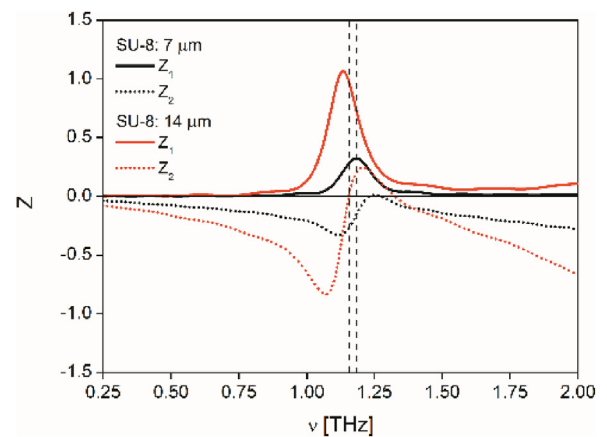


**Fig. 4.** Wave impedance obtained from numerical simulations for a reflective TMA with a SU-8 thickness of 7  $\mu\text{m}$  ( $Z_1$  – black solid line,  $Z_2$  – black dotted line) and for a reflective perfect TMA with a SU-8 thickness of 14  $\mu\text{m}$  ( $Z_1$  – red solid line,  $Z_2$  – red dotted line).

## 6. Transmissive terahertz metamaterial absorbers

Figure 5 shows the experimental and simulated absorption of the transmissive TMAs. The experimental spectrum was obtained for the TMA with a 550  $\mu\text{m}$  thick Si substrate and a 7  $\mu\text{m}$  thick SU-8 layer. The simulated spectra refer to a unit cell with the same dimensions as the manufactured TMA, as well as two other TMA cells with a much thinner Si substrate (12  $\mu\text{m}$  thick in each case); the thickness of the SU-8 layer in these other two cells was 7  $\mu\text{m}$  and 14  $\mu\text{m}$ , respectively. The absorption peaks for all three cases where the SU-8 thickness was 7  $\mu\text{m}$  are very similar to each other regardless of whether the assumed thickness of the Si is 550  $\mu\text{m}$  or 12  $\mu\text{m}$ . The peaks in the experimental and simulated absorption spectra occur at 1.19 THz and 1.17 THz, respectively. The corresponding peak heights are of 0.75 and 0.78. The peaks differ substantially from each other in half-width, which is about 0.30 THz for the experimental spectrum and 0.20 THz for the two simulated spectra. On the other hand, the absorption peak for the TMA with the thicker SU-8 layer (14  $\mu\text{m}$ ) is shifted toward lower frequencies, and the maximum occurs at 0.98 THz. Maximum absorption of this peak

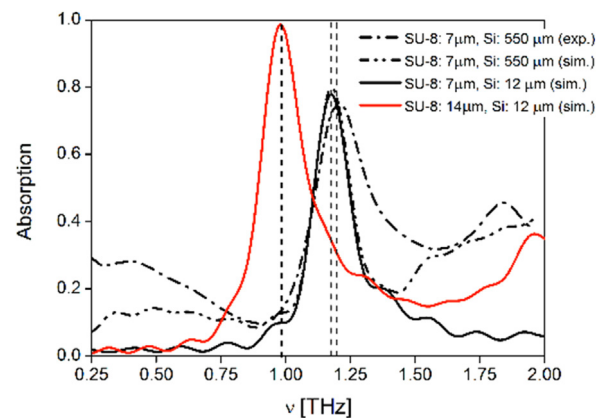


**Fig. 5.** Absorption spectra of four different transmissive TMAs with various thicknesses of the Si substrate and the SU-8 layer. The two dashed curves are for the experimentally measured (manufactured) sample (black dash-dotted line) and the numerically simulated sample (black dash-double-dotted line) where the thicknesses of Si and SU-8 were 550  $\mu\text{m}$  and 7  $\mu\text{m}$ , respectively, in each case. Two solid curves are for the numerically simulated samples with the 12  $\mu\text{m}$  thick Si substrates, where the thickness of the SU-8 layer was either 7  $\mu\text{m}$  (black solid line), or 14  $\mu\text{m}$  (red solid line).

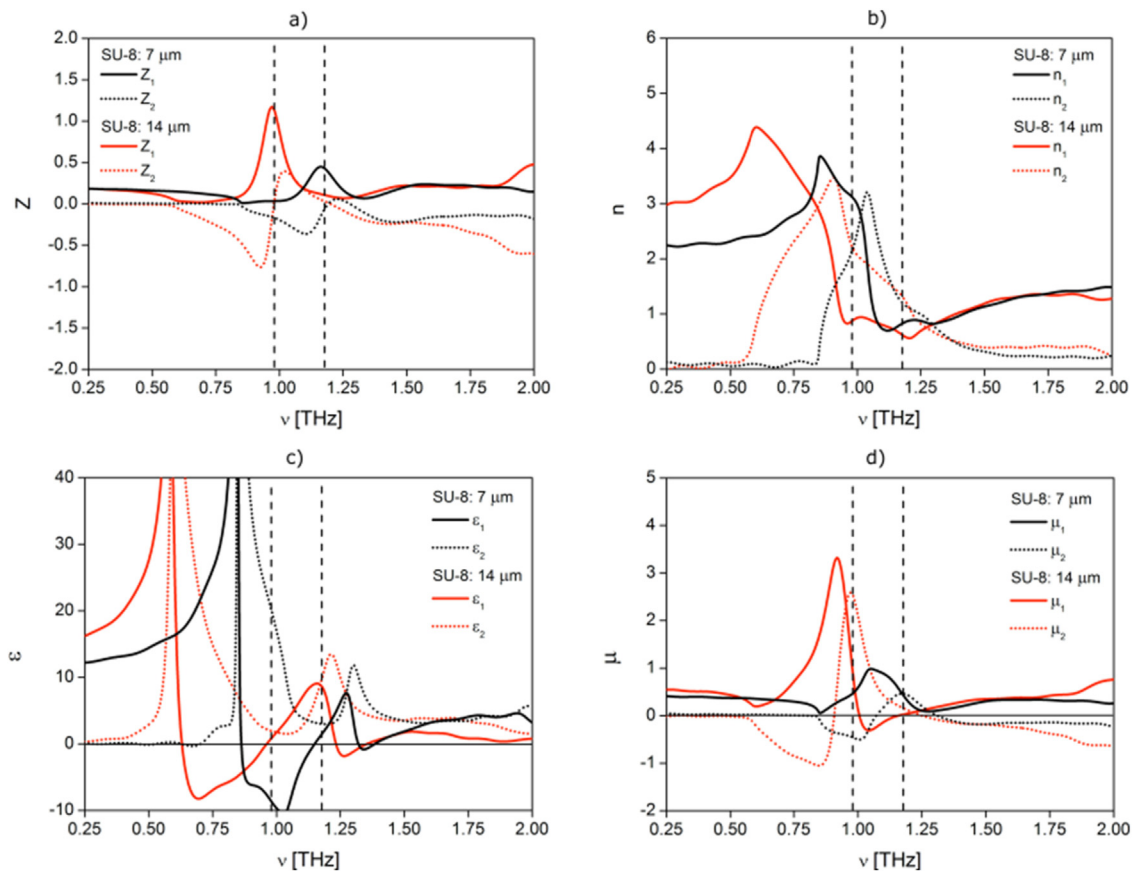


**Fig. 6.** Real (solid lines) and imaginary (dotted lines) parts of the wave impedance a), refractive index b), permittivity c), and permeability d) for a transmissive non-perfect TMA with a SU-8 layer thickness of 7  $\mu\text{m}$  (black lines) and for a perfect TMA with a SU-8 layer thickness of 14  $\mu\text{m}$  (red lines). The thickness of the Si substrate is of 12  $\mu\text{m}$  in both cases.

is close to unity, which satisfies the condition of perfect absorption. The half width of this peak is equal to 0.21 THz.

Figures 6a)–6d) present the real and imaginary parts of the wave impedance, refractive index, permittivity, and permeability calculated from the numerically simulated Sparameters for the transmissive non-perfect and the perfect TMAs. The effective permittivity and permeability of the presented metamaterial result both from the electromagnetic properties of the dielectric (SU-8), metal (Al) and semiconductor (high-resistivity Si) materials used, as well as geometric parameters of the elementary unit (layer thickness, characteristic pattern of the metal structure). Substitution of these materials for others is usually associated with a change in the transmission, reflection and absorption properties of the metamaterial. In particular, this applies to metals for which conductivity, permeability dispersion, and permittivity in the THz range are important [38,39]. However, as can be seen in Fig. 6, the effective permittivity and permeability of the presented metamaterial as a frequency functions are significantly different from the relevant characteristics of the materials used. The presented characteristics (effective permittivity and permeability) are primarily a consequence of the shape and size of the elements forming the unit cell of the metamaterial, and to a lesser extent, electromagnetic parameters of the materials used.

For the simulated non-perfect TMA, the thickness of the SU-8 is the same as in the fabricated sample (7  $\mu\text{m}$ ), whereas for the perfect TMA it is assumed to be equal to 14  $\mu\text{m}$ . It can be seen in Fig. 6a) and 6b) that for the perfect TMA,  $Z_1 = 1$ ,  $Z_2 = 0$ , and  $n_2 = 2$  at the absorption maximum (0.98 THz). For the non-perfect TMA,  $Z_1 = 0.43$  (i.e.,  $< 1$ ), at the absorption maximum (1.17 THz), while  $Z_2$  is almost equal to zero. In this case,  $n_2$  is about 1.18.

Absorption of the metamaterial unit cell can be analysed as a function of frequency, based on the formula describing density of electromagnetic field power that is absorbed in a material [40,41]:

$$P(\nu) = P_e(\nu) + P_m(\nu) = \frac{1}{2} \nu \epsilon_2 \epsilon_0 |E|^2 + \frac{1}{2} \nu \mu_2 \mu_0 |H|^2, \quad (3)$$

where  $P_e(\nu)$  and  $P_m(\nu)$  describe the electric and magnetic parts of the electromagnetic power density,  $|E|$  and  $|H|$  are the electric and magnetic field amplitudes,  $\epsilon_2$  and  $\mu_2$  are the imaginary parts of the permittivity and permeability, and  $\epsilon_0$  and  $\mu_0$  are the electric and magnetic constants of free space.

It follows from Eq. (3) that the process of frequency-dependent absorption of electromagnetic field energy is directly related to the imaginary parts of the electric permittivity,  $\epsilon_2$ , and the magnetic permeability,  $\mu_2$ . In the non-perfect TMA, the energy associated with the electric field of the wave is intensively absorbed in the frequency range from 0.80 THz up to about 1.10 THz, as evidenced by the large positive values of  $\epsilon_2$  [Fig. 6c)]. Simultaneously, in this frequency range, the magnetic field energy in this TMA is intensively scattered, which is related to the negative values of  $\mu_2$  [Fig. 6d)]. The relatively low total absorption of the non-perfect TMA is a result of the competition between these two processes. For the non-perfect TMA, the imaginary part of the magnetic permeability,  $\mu_2$ , has a local maximum at 1.17 THz with the peak value greater than zero. This frequency coincides with the absorption maximum of the non-perfect TMA (Fig. 5). The local maximum of the imaginary part of the permittivity,  $\epsilon_2$ , occurring at 1.35 THz is responsible for the increase of the long wavelength shoulder in the absorption peak. For the perfect TMA, the position of the absorption maximum at 0.98 THz is correlated with the position of the maximum of  $\mu_2$  [Fig. 6d)]. Since

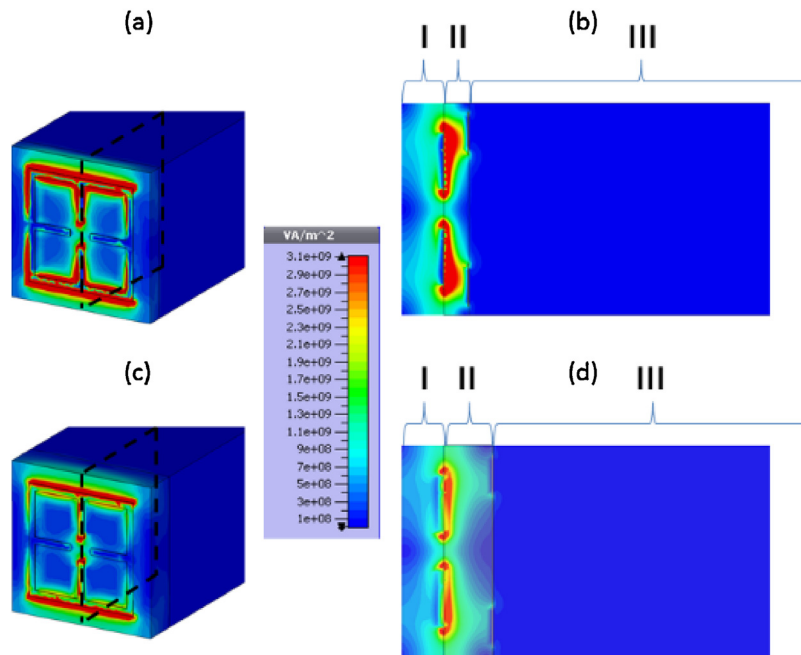


**Fig. 7.** Power flow distribution inside and outside the metamaterial unit cell of a transmissive non-perfect TMA with a 7  $\mu\text{m}$  thick SU-8 layer (a, b) and a perfect TMA with a 14  $\mu\text{m}$  thick SU-8 layer (c, d); the thickness of the Si substrate equals 50  $\mu\text{m}$  in both cases (CST Microwave Studio<sup>®</sup>).

$\mu_2$  is positive at this frequency, the absorption of the perfect TMA is primarily the result of absorption of the magnetic field energy in the medium. The absorption of the electric field energy, which is associated with the local maximum of  $\epsilon_2$  at 1.23 THz [Fig. 6c], contributes to the increase of the long wavelength shoulder in the absorption peak of the perfect TMA.

## 7. Power flow distribution

The power flow distributions inside and outside the unit cells of the transmissive non-perfect and the perfect TMAs, obtained from numerical simulations, are presented in Fig. 7. The thicknesses of the SU-8 layers are equal to 7  $\mu\text{m}$  and 14  $\mu\text{m}$  for non-perfect and perfect absorbers, respectively. In order to minimize the contribution of interference effects in the Si substrate to the results of numerical simulations, the thickness of the Si substrate is assumed to be of 50  $\mu\text{m}$ . In the simulation, the electromagnetic wave extends perpendicular to the surface of the TMA and has its electric field vector parallel to the sides of the outer metal structures in the unit cell. The ports' areas are equal to the area of the unit cell surface. Power flow distributions in the TMAs are simulated at frequencies of 1.17 THz and 0.98 THz, corresponding to the absorption maxima of the non-perfect TMA and the perfect TMA, respectively. Power flow of the incident wave at the input port is set equal to 1 W.

For ease of discussion, the space included in the simulations is arbitrarily divided into three zones. The first zone (zone I) covers the outer metal layer and 12  $\mu\text{m}$  of free space in front of it. The second zone (zone II) includes the SU-8 layer and the inner metal layer. The third zone (zone III) comprises the Si substrate (50  $\mu\text{m}$ ) and 12  $\mu\text{m}$  of free space behind it. This formal separation is presented in the cross-section of the unit cell of the TMA [Figs. 7(b) and 7(d)]. The cross-section is displayed along a plane that is parallel both to the electric field vector and the wave vector of the incident wave. As can be seen in Figs. 7(b) and 7(d) for both the non-perfect TMA and the perfect TMA, power flow is highly inhomogeneous in the vicinity of the outer metal pattern (zones I and II). This inhomogeneity is the result of both significant field enhancement near outer metal layer and intensive absorption of electromagnetic waves in this region.

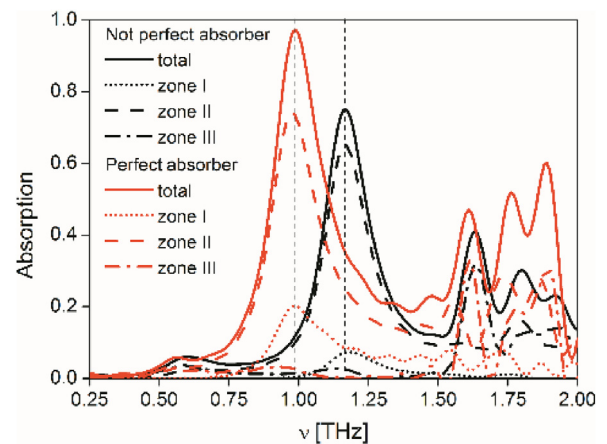


**Fig. 8.** Absorption in a transmissive non-perfect TMA (black lines) and in a perfect TMA (red lines): total absorption in unit cell (solid lines), zone I (dotted lines), zone II (dashed lines), and zone III (dash dotted lines).

By contrast, the power flow in the Si substrate (zone III) is relatively low and homogenous, even in close proximity to the inner metal layer.

The absorption of the electromagnetic field for the transmissive non-perfect and the perfect TMAs in zones I, II, and III is presented in Fig. 8. The absorption in each zone is calculated as the quotient of the difference between the power flows at two opposite boundary surfaces of a given zone divided by the power flow at the incident port (equal to 1 W). It can be seen that the absorption in zones I and II contributes the most to the total absorption at the peak. These absorptions are equal to 75% and 96%, for the non-perfect TMA and the perfect TMA, respectively. For the non-perfect TMA and the perfect TMA, about 65% and 74%, respectively, of the total power of the incident wave is absorbed in zone II. It is evident that the dielectric layer plays the most significant role in the process of narrowband electromagnetic energy absorption in the TMAs. Power absorbed in zone I, which is about 8% and 20% of the total power of the incident wave for the non-perfect TMA and the perfect TMA,

correspondingly, is much less but also important. It should be noted that the influence of the Si substrate (zone III) on the narrowband absorption is negligibly small. The simulation results indicate that the greatest contribution to the absorption in the investigated TMAs arises from dielectric losses in the SU-8 layers. An analogous conclusion was drawn by Landy *et al.*, who analysed a different planar metamaterial absorber in the GHz range [42].

## 8. Conclusions

We have investigated reflective and transmissive planar terahertz metamaterial absorbers with a metal-organic dielectric-metal layered structure. Dielectric layers from organic materials such as SU-8 epoxy resist used by us are a serious alternative to inorganic dielectrics such as  $\text{Al}_2\text{O}_3$ , for example. SU-8 epoxy resist is well known as a structural material for MEMS devices. Application of SU-8 allows simplification of the process of producing TMAs and significantly reduces fabrication costs. Experimental tests have shown that in the case of the SU-8 dielectric spacer, the use of mask photolithography allows to fabricate TMA with the size of the smallest resonator details of about  $2\ \mu\text{m}$ . Such accuracy is sufficient for the fabrication of metamaterial absorbers having characteristic resonances in the terahertz and mid-infrared ranges. It should be mentioned here that because of plasmonic resonance resides in these spectral ranges, graphene is a promising material for various applications [43]. Plasmonic structures using graphene are now intensively studied. Numerical simulations, as well as analytical calculations indicate that metal structures in the electromagnetic absorbers, which are, in particular, polarization insensitive, can be replaced with graphene structures [44,45]. A practical matter to solve in this case would be the possibility of preparing very thin layers of organic dielectrics, such as SU-8, on graphene structures.

Our goal was to investigate the physical characteristics related to the absorption and scattering of electromagnetic energy in TMAs with SU-8 dielectric separator. We have fabricated the reflective and transmissive planar TMAs with a  $7\ \mu\text{m}$  thick SU-8 layer and have shown that these TMAs had absorption characteristics that were substantially consistent with the results of the numerical simulations. In the simulations, we have modified the mathematical formulas defining S-parameters to take into account port distances from the outside surfaces of the absorbers. Especially good agreement between experimental results and numerical simulations was obtained for the reflective TMAs, for which there was no need to consider the thick substrate influence on the absorption characteristics. For the transmissive TMAs with the identical elementary resonator in the outer plane and of the same thickness of the SU-8 dielectric layer, the frequency of the absorption band maximum was very close to the peak absorption frequency of the corresponding reflective TMA. Compatibility of numerical simulations with the results of experiments was the justification for the use of numerical simulations to determine the parameters of the perfect TMAs ( $A=1$ ). The simulations for unit cells of the investigated reflective and transmissive TMAs revealed that in both cases the perfect absorption occurred for  $14\ \mu\text{m}$  thick SU-8 layers.

Using S-parameters, we have calculated the effective wave impedance, refractive index, permittivity, and permeability as functions of frequency for transmissive TMAs, both perfect and non-perfect. We have interpreted the total absorption in TMA as a result of energy dissipation of the electrical and magnetic components of the field. Positive values of imaginary parts of permittivity and permeability were related to the absorption of the electromagnetic field in the material, while negative values of these parameters were responsible for the scattering. Based on the imaginary parts of the permittivity and permeability, we have calculated the absorption of the electromagnetic field in three characteris-

tic zones of the transmissive TMA unit cell. We have shown that more than two-thirds of the total electromagnetic wave absorption occurred in the zone containing the SU-8 dielectric layer. Numerical simulations have confirmed that the dielectric characteristics of materials in the terahertz range have a significant impact on the absorption properties of TMAs with the metal-organic dielectric-metal structure.

## Author's statement

The authors' individual contributions to the manuscript "SU-8 based planar metamaterials with fourfold symmetry as selective terahertz absorbers" are as follows:

### 1) Bartłomiej Grześkiewicz

Conceptualization; data curation; formal analysis; investigation; methodology; visualization; writing – discussion of original draft, drawings.

### 2) Andrzej Sierakowski

Investigation; methodology.

### 3) Jacek Marczewski

Resources; supervision; validation.

### 4) Norbert Pałka

Resources; supervision; validation; writing – review and editing.

### 5) Eryk Wolarz

Conceptualization; formal analysis; funding acquisition; methodology; project administration; resources; supervision; validation; writing – original draft; writing – review and editing.

## Declarations of interest

None.

## Acknowledgements

This work was funded by the Polish Ministry of Science and Higher Education through the Poznan University of Technology, grant no. 06/65/DSPB/5181.

## References

- [1] D.R. Smith, W.J. Padilla, D.C. Vier, S.C. Nemat-Nasser, S. Schultz, Composite medium with simultaneously negative permeability and permittivity, *Phys. Rev. Lett.* 84 (2000) 4184–4187, <http://dx.doi.org/10.1103/PhysRevLett.84.4184>.
- [2] H. Tao, W.J. Padilla, X. Zhang, R.D. Averitt, Recent progress in electromagnetic metamaterial devices for terahertz applications, *IEEE J. Sel. Top. Quantum Electron.* 17 (2011) 92–101, <http://dx.doi.org/10.1109/JSTQE.2010.2047847>.
- [3] W.J. Padilla, M.T. Aronsson, C. Highstrete, M. Lee, A.J. Taylor, R.D. Averitt, Electrically resonant terahertz metamaterials: theoretical and experimental investigations, *Phys. Rev. B* 75 (2007) 041102, <http://dx.doi.org/10.1103/PhysRevB.75.041102>.
- [4] C.M. Watts, X. Liu, W.J. Padilla, Metamaterial electromagnetic wave absorbers, *Adv. Mater.* 24 (2012) OP98–OP120, <http://dx.doi.org/10.1002/adma.201200674>.
- [5] O. Paul, C. Imhof, B. Reinhard, R. Zengerle, R. Beigang, Negative index bulk metamaterial at terahertz frequencies, *Opt. Express* 16 (2008) 6736–6744, <http://dx.doi.org/10.1364/OE.16.006736>.
- [6] H. Tao, N.I. Landy, C.M. Bingham, X. Zhang, R.D. Averitt, W.J. Padilla, A metamaterial absorber for the terahertz regime: design, fabrication and characterization, *Opt. Express* 16 (2008) 7181–7188, <http://dx.doi.org/10.1364/OE.16.007181>.
- [7] H. Tao, C.M. Bingham, A.C. Strikwerda, D. Pilon, D. Shrekenhamer, N.I. Landy, K. Fan, X. Zhang, W.J. Padilla, R.D. Averitt, Highly flexible wide angle of incidence terahertz metamaterial absorber: design, fabrication, and characterization, *Phys. Rev. B* 78 (2008) 241103, <http://dx.doi.org/10.1103/PhysRevB.78.241103>.
- [8] N.I. Landy, C.M. Bingham, T. Tyler, N. Jokerst, D.R. Smith, W.J. Padilla, Design, theory, and measurement of a polarization-insensitive absorber for terahertz imaging, *Phys. Rev. B* 79 (2009) 125104, <http://dx.doi.org/10.1103/PhysRevB.79.125104>.

- [9] H. Kong, G. Li, Z. Jin, G. Ma, Z. Zhang, C. Zhang, Polarization-independent metamaterial absorber for terahertz frequency, *J. Infrared Milli Terahz Waves* 33 (2012) 649–656, <http://dx.doi.org/10.1007/s10762-012-9906-x>.
- [10] B. Grześkiewicz, A. Sierakowski, J. Marczewski, N. Pałka, E. Wolarz, Polarization-insensitive metamaterial absorber of selective response in terahertz frequency range, *J. Opt.* 16 (2014) 105104, <http://dx.doi.org/10.1088/2040-8978/16/10/105104>.
- [11] Q.-Y. Wen, H.-W. Zhang, Y.-S. Xie, Q.-H. Yang, Y.-L. Liu, Dual band terahertz metamaterial absorber: design, fabrication, and characterization, *Appl. Phys. Lett.* 95 (2009) 241111, <http://dx.doi.org/10.1063/1.3276072>.
- [12] H. Tao, C.M. Bingham, D. Pilon, K. Fan, A.C. Strikwerda, D. Shrekenhamer, W.J. Padilla, X. Zhang, R.D. Averitt, A dual band terahertz metamaterial absorber, *J. Phys. D Appl. Phys.* 43 (2010) 225102, <http://dx.doi.org/10.1088/0022-3727/43/22/225102>.
- [13] B.-X. Wang, X. Zhai, G.-Z. Wang, W.-Q. Huang, L.-L. Wang, A novel dual-band terahertz metamaterial absorber for a sensor application, *J. Appl. Phys.* 117 (2015) 014504, <http://dx.doi.org/10.1063/1.4905261>.
- [14] X. Shen, T.J. Cui, J. Zhao, H.F. Ma, W.X. Jiang, H. Li, Polarization-independent wide-angle triple-band metamaterial absorber, *Opt. Express* 19 (2011) 9401–9407, <http://dx.doi.org/10.1364/OE.19.009401>.
- [15] R. Yahiaoui, S. Tan, L. Cong, R. Singh, F. Yan, W. Zhang, Multispectral terahertz sensing with highly flexible ultrathin metamaterial absorber, *J. Appl. Phys.* 118 (2015) 083103, <http://dx.doi.org/10.1063/1.4929449>.
- [16] I. Al-Naib, Y. Yang, M.M. Dignam, W. Zhang, R. Singh, Ultra-high Q even eigenmode resonance in terahertz metamaterials, *Appl. Phys. Lett.* 106 (2015) 011102, <http://dx.doi.org/10.1063/1.4905478>.
- [17] S. Liu, H. Chen, T.J. Cui, A broadband terahertz absorber using multi-layer stacked bars, *Appl. Phys. Lett.* 106 (2015) 151601, <http://dx.doi.org/10.1063/1.4918289>.
- [18] S. Yin, J. Zhu, W. Xu, W. Jiang, J. Yuan, G. Yin, L. Xie, Y. Ying, Y. Ma, High-performance terahertz wave absorbers made of silicon-based metamaterials, *Appl. Phys. Lett.* 107 (2015) 073903, <http://dx.doi.org/10.1063/1.4929151>.
- [19] J. Zhu, Z. Ma, W. Sun, F. Ding, Q. He, L. Zhou, Y. Ma, Ultra-broadband terahertz metamaterial absorber, *Appl. Phys. Lett.* 105 (2014) 021102, <http://dx.doi.org/10.1063/1.4890521>.
- [20] G. Duan, J. Schalch, X. Zhao, J. Zhang, R.D. Averitt, X. Zhang, Analysis of the thickness dependence of metamaterial absorbers at terahertz frequencies, *Opt. Express* 26 (2018) 2242–2251, <http://dx.doi.org/10.1364/OE.26.002242>.
- [21] R. Kowderdzij, M. Olifierczuk, J. Parka, Thermally induced tunability of a terahertz metamaterial by using a specially designed nematic liquid crystal mixture, *Opt. Express* 26 (2018) 2443–2452, <http://dx.doi.org/10.1364/OE.26.002443>.
- [22] S.J. Park, J.T. Hong, S.J. Choi, H.S. Kim, W.K. Park, S.T. Han, J.Y. Park, S. Lee, D.S. Kim, Y.H. Ahn, Detection of microorganisms using terahertz metamaterials, *Sci. Rep.* 4 (2014) 4988, <http://dx.doi.org/10.1038/srep04988>.
- [23] M. Chen, L. Singh, N. Xu, R. Singh, W. Zhang, L. Xie, Terahertz sensing of highly absorptive water-methanol mixtures with multiple resonances in metamaterials, *Opt. Express* 25 (2017) 14089–14097, <http://dx.doi.org/10.1364/OE.25.014089>.
- [24] J.F. Federici, B. Schulkin, F. Huang, D. Gary, R. Barat, F. Oliveira, D. Zimdars, THz imaging and sensing for security applications—explosives, weapons and drugs, *Semicond. Sci. Technol.* 20 (2005) S266, <http://dx.doi.org/10.1088/0268-1242/20/7/018>.
- [25] L. Viti, D. Coquillat, D. Ercolani, L. Sorba, W. Knap, M.S. Vitiello, Nanowire Terahertz detectors with a resonant four-leaf-clover-shaped antenna, *Opt. Express* 22 (2014) 8996–9003, <http://dx.doi.org/10.1364/OE.22.008996>.
- [26] J. Grant, I. Escorcía-Carranza, C. Li, I.J.H. McCrindle, J. Gough, D.R.S. Cumming, A monolithic resonant terahertz sensor element comprising a metamaterial absorber and micro-bolometer, *Laser Photon. Rev.* 7 (2013) 1043–1048, <http://dx.doi.org/10.1002/lpor.201300087>.
- [27] S.A. Ramakrishna, T.M. Grzegorzczak, *Physics and Applications of Negative Refractive Index Materials*, CRC Press, 2008 (Accessed February 23, 2018) <https://www.crcpress.com/Physics-and-Applications-of-Negative-Refractive-Index-Materials/Ramakrishna-Grzegorzczak/p/book/9781420068757>.
- [28] D.R. Smith, D.C. Vier, T. Koschny, C.M. Soukoulis, Electromagnetic parameter retrieval from inhomogeneous metamaterials, *Phys. Rev. E* 71 (2005) 036617, <http://dx.doi.org/10.1103/PhysRevE.71.036617>.
- [29] X. Chen, T.M. Grzegorzczak, B.-I. Wu, J. Pacheco, J.A. Kong, Robust method to retrieve the constitutive effective parameters of metamaterials, *Phys. Rev. E* 70 (2004) 016608, <http://dx.doi.org/10.1103/PhysRevE.70.016608>.
- [30] D.R. Smith, S. Schultz, P. Markoš, C.M. Soukoulis, Determination of effective permittivity and permeability of metamaterials from reflection and transmission coefficients, *Phys. Rev. B* 65 (2002) 195104, <http://dx.doi.org/10.1103/PhysRevB.65.195104>.
- [31] Z. Liu, P.W.C. Hon, A.A. Tavallae, T. Itoh, B.S. Williams, Terahertz composite right-left handed transmission-line metamaterial waveguides, *Appl. Phys. Lett.* 100 (2012) 071101, <http://dx.doi.org/10.1063/1.3684250>.
- [32] D. Grbovic, F. Alves, B.T. Kearney, B. Waxer, R. Perez, G. Omicini, Metal-organic hybrid resonant terahertz absorbers with SU-8 photoresist dielectric layer, *J. Micro/Nanolith. MEMS MOEMS* 12 (2013) 041204, <http://dx.doi.org/10.1117/1.JMM.12.4.041204>.
- [33] H. Lorenz, M. Despont, N. Fahrni, N. LaBianca, P. Renaud, P. Vettiger, SU-8: a low-cost negative resist for MEMS, *J. Micromech. Microeng.* 7 (1997) 121, <http://dx.doi.org/10.1088/0960-1317/7/3/010>.
- [34] Y. Tian, X. Shang, Y. Wang, M.J. Lancaster, Investigation of SU8 as a structural material for fabricating passive millimeter-wave and terahertz components, *J. Micro/Nanolith. MEMS MOEMS* 14 (2015) <https://doi.org/10.1117/1.JMM.14.4.044507>.
- [35] J. Dai, J. Zhang, W. Zhang, D. Grischkowsky, Terahertz time-domain spectroscopy characterization of the far-infrared absorption and index of refraction of high-resistivity, float-zone silicon, *J. Opt. Soc. Am. B* 21 (2004) 1379–1386, <http://dx.doi.org/10.1364/JOSAB.21.001379>.
- [36] S. Arscott, F. Garet, P. Mounaix, L. Duvillearet, J.L. Coutaz, D. Lippens, Terahertz time-domain spectroscopy of films fabricated from SU-8, *Electron. Lett.* 35 (1999) 243–244, <http://dx.doi.org/10.1049/el:19990146>.
- [37] S. Lucyszyn, Comment: terahertz time-domain spectroscopy of films fabricated from SU-8, *Electron. Lett.* 37 (2001) 1267, <http://dx.doi.org/10.1049/el:20010847>.
- [38] A. Ishikawa, T. Tanaka, Negative magnetic permeability of split ring resonators in the visible light region, *Opt. Commun.* 258 (2006) 300–3005, <http://dx.doi.org/10.1016/j.optcom.2005.07.076>.
- [39] R. Singh, A.K. Azad, J.F. O'Hara, A.J. Taylor, W. Zhang, Effect of metal permittivity on resonant properties of terahertz metamaterials, *Optics Lett.* 33 (2008) 1506–1508, <http://dx.doi.org/10.1364/OL.33.001506>.
- [40] L.D. Landau, E.M. Lifshits, *Electrodynamics of Continuous Media*, Pergamon, 1984.
- [41] J. Hao, L. Zhou, M. Qiu, Nearly total absorption of light and heat generation by plasmonic metamaterials, *Phys. Rev. B* 83 (2011) 165107, <http://dx.doi.org/10.1103/PhysRevB.83.165107>.
- [42] N.I. Landy, S. Sajuyigbe, J.J. Mock, D.R. Smith, W.J. Padilla, Perfect metamaterial absorber, *Phys. Rev. Lett.* 100 (2008) 207402, <http://dx.doi.org/10.1103/PhysRevLett.100.207402>.
- [43] T. Low, P. Avouris, Graphene plasmonics for terahertz to mid-infrared applications, *ACS Nano* 8 (2014) 1086–1101, <http://dx.doi.org/10.1021/nn406627u>.
- [44] S.-X. Xia, X. Zhai, Y. Huang, J.-Q. Liu, L.-L. Wang, S.-C. Wen, Multi-band perfect plasmonic absorptions using rectangular graphene gratings, *Opt. Lett.* 42 (2017) 3052–3055, <http://dx.doi.org/10.1364/OL.42.003052>.
- [45] S.-X. Xia, X. Zhai, L.-L. Wang, S.-C. Wen, Plasmonically induced transparency in double-layered graphene nanoribbons, *Photon. Res. J.* 6 (2018) 692–702, <http://dx.doi.org/10.1364/PRJ.6.000692>.